PHYSICAL REVIEW D VOLUME 24, NUMBER 7 1 OCTOBER 1981

Measurements of charged-pion production from neutron-proton collisions at 790 MeV

W. Thomas,* R. Carlini,† C. Cassapakis,‡ B. Dieterle, J. Donahue, C. Leavitt, T. Rupp,§ and D. Wolfe
Department of Physics and Astronomy, University of New Mexico, Albuquerque, New Mexico 87131

M. L. Evans,† G. Glass, Mahavir Jain,† and L. Northcliffe
Texas A&M University, College Station, Texas 77843

B. Bonner and J. Simmons
Los Alamos Scientific Laboratory, Los Alamos, New Mexico 87545
(Received 17 July 1980)

Pion energy spectra from the reactions $np \to nn\pi^+$ and $np \to pp\pi^-$ were measured as a function of the angle at 790 MeV. The angular distribution in the np center-of-momentum system was given by $[(123.1\pm2.7)+(88.3\pm4.9)\cos^2\theta^*]$ μb/sr. The total cross section for each reaction was found to be 1.92 ± 0.20 mb. Evidence for $T=0$ pion production was observed in shape differences between the positive- and negative-pion spectra. However, it was shown that pions are preferentially produced by nucleons in a

I. INTRODUCTION

This paper describes an experiment performed at the Los Alamos Meson Physics Facility (LAMPF) in which a 790-MeV neutron beam was used to initiate the following reactions:

$$n+p \to n+n+\pi^+ , \tag{1}$$

$$n+p \to p+p+\pi^- . \tag{2}$$

The resulting pion spectra were measured at ten different angles with a multiwire-proportional-chamber spectrometer.

Studies involving neutron-proton reactions are necessary to obtain data on the $T=0$ nucleon-nucleon isotopic-spin state. It is possible to extract information on the $T=0$ interaction by appropriately combining np and pp (or nn) data. For example, consider the total cross section for all single-pion production (π^+,π^-,π^0) from $T=0$ neutron-proton interactions. This cross section [$\sigma(T=0)$] can be expressed as follows:

$$\sigma(T=0)=3\sigma_{01} , \tag{3a}$$

where

$$\sigma_{01}=2\sigma(np \to NN\pi^\pm)-\sigma_{11} ,$$

$$\sigma(np \to NN\pi^\pm)=\sigma(np \to pp\pi^-)=\sigma(np \to nn\pi^+) , \tag{3b}$$

and

$$\sigma_{11}=\sigma(pp \to pp\pi^0) . \tag{3c}$$

The subscripts on the partial cross sections σ_{01} and σ_{11} identify, in order, the isotopic spins of the initial- and final-state nucleons. The neglect of Coulomb effects, the neutron-proton mass difference, and the π^0-$\pi^\pm$ mass difference introduce uncertainties in these relationships. However, the corrections to these relationships are estimated to be no more than a few percent.[1]

The Mandelstam model[2] has been used to describe single-pion production from threshold to about 800 MeV. One of the basic assumptions of this model is that the outgoing pion and one of the nucleons form the $\Delta(1232)$ resonant state. In this case, isospin conservation requires that the colliding nucleons be in a $T=1$ state, which means that the total pion-production amplitudes should be front-back symmetic in the center-of-momentum system (c.m.s.) and that $\sigma(T=0)$ should be zero. However, results from previous experiments[3-7] concerning reactions (1) and (2) indicate the existence of $T=0$ amplitudes. Specifically, Yodh[3] found substantial differences between the π^+ and π^- energy spectra and angular distributions at 400 MeV, a strong indication of interfering $T=0$ and $T=1$ amplitudes. Handler[4] also found differences between the pion angular distributions near 400

MeV. The actual value of $\sigma(T=0)$, as calculated from relations (3a)–(3c), has been shown in several cases to be significantly different from zero. However, it should be noted that these experiments, which were typically based on less than ~ 1000 events, had poor statistical accuracy and poor pion-energy definition. In addition, the energy of each neutron beam was very broadly distributed, having a full width at half maximum (FWHM) of at least 20% of the quoted energy. The last situation makes it especially difficult to determine $\sigma(T=0)$, since σ_{11} varies rapidly with energy up to about 800 MeV and $\sigma(T=0)$ is thus very sensitive to the "effective" neutron energy. The neutron beam used in the present experiment was very nearly monoenergetic (~ 18 MeV FWHM) and thus provides us with a distinct advantage over the previous experiments. We were also able to achieve improved statistical accuracy ($\sim 100\,000$ events) and considerably improved pion energy resolution.

Our data provide another test for nonresonant pion production. In addition, we can test pion-production models in an energy region which has traditionally been difficult to describe theoretically. In particular, the Mandelstam model probably breaks down around 700–800 MeV,[8] due to the failure of two assumptions made in this model, namely that only a few partial waves are present and that the production matrix elements are independent of energy. The one-pion-exchange model of Ferrari and Selleri,[9] approximately valid from $\sim 800-1500$ MeV, apparently fails in the same region due to the neglect of nucleon-nucleon final-state interactions. It is worth noting that a phenomenological model developed recently by Stephenson, Gibbs, and Gibson, has been applied with good success to 0° neutron spectra from the reaction $pp \rightarrow np\pi^+$ at 647, 777, and 805 MeV.[10] This model includes an NN final-state interaction and S- and P-wave pion-nucleon phase shifts at the π-N scattering vertex. It is anticipated that a future paper will provide comparisons of this model with (1) the present data and (2) a recent 800-MeV experiment concerning the reaction $pp \rightarrow np\pi^+$ which yielded data on the angular variation of the neutron-energy spectrum.[11]

II. EXPERIMENTAL METHOD

A. Outline of the experiment

This experiment was performed at the Nucleon Physics Laboratory located at LAMPF. An 800-MeV proton beam was focused onto a liquid-deuterium (LD_2) target where neutrons were produced via the reaction $pd \rightarrow nX$. Bending magnets located behind the LD_2 target diverted the remaining proton beam and other charged particles into a beam stop [Fig. 1(a)]. Neutrons produced at 0° with respect to the incident proton beam were selected by means of a collimator also shown in Fig. 1(a). This collimator, 3.66 m in length, was constructed from a 155-mm gun barrel surrounded by large amounts of concrete and steel shielding. Annular lead and steel inserts placed in the gun barrel reduced the collimator diameter to 2.54 cm. A 6.35-cm-thick lead plug was placed near the downstream end of the collimator to reduce the flux of the beam-associated γ rays. This lead had essentially no effect on the shape of the 0° neutron spectrum, although it did reduce the intensity by approximately 20 percent, while the γ rays were attenuated by a factor greater than 20.

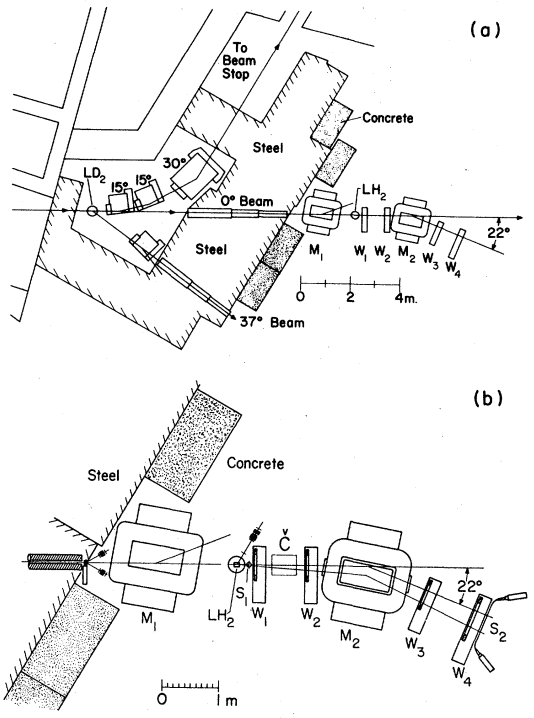

FIG. 1. (a) Experimental arrangement. (b) Spectrometer layout.

After exiting the collimator, the neutrons passed through a sweep magnet (M_1) which served to remove residual charged particles from the beam. Located downstream from M_1 was a liquid-hydrogen target (LH_2), in which the np interactions took place. The liquid hydrogen was contained in a cylindrical mylar flask 13.2 cm long by

10.15 cm, and had an areal density in the beam direction of 0.94 gm/cm^2. The liquid-hydrogen density varied by about 1% rms because of 20% pressure fluctuations in the target flask. Pions and other charged particles produced in the LH_2 target were momentum analyzed as a function of angle with the multiwire-proportional-chamber (MWPC) spectrometer shown in Fig. 1(b). This spectrometer will be described more fully in a later section.

B. Neutron beam

The 0° neutron-beam spectrum produced through the reaction $pd \rightarrow nX$ at 800-MeV incident proton energy is shown in Fig. 2.[12] The narrow peak ($\sim$18 MeV FWHM) close to the incident proton energy is due to quasielastic charge-exchange scattering involving the incident proton and the deuteron neutron. The broad peak centered around 450 MeV contains neutrons emitted during inelastic *pd* collisions. The displacement ($\sim$7 MeV) between the high-energy-peak centroid and incident proton energy is caused by the dynamics of the deuteron breakup process. Proton-energy losses in the LD_2 target during the present experiment shifted this peak slightly further, to about 790 MeV. The majority of the pions detected in this experiment were produced by neutrons having energies within the limits of the high-energy peak. The intensity of these neutrons on the LH_2 target varied from $\sim 4\times 10^5$/sec to $\sim 5\times 10^6$/sec. These rates were determined by the quasielastic *pd* cross section ($\sim$30 mb/sr), the LD_2 target density (1.8 gm/cm^2), the collimator solid angle (9.1×10^{-6} sr), and the incident-proton-beam current ($\frac{1}{2}$ to 6 μA).

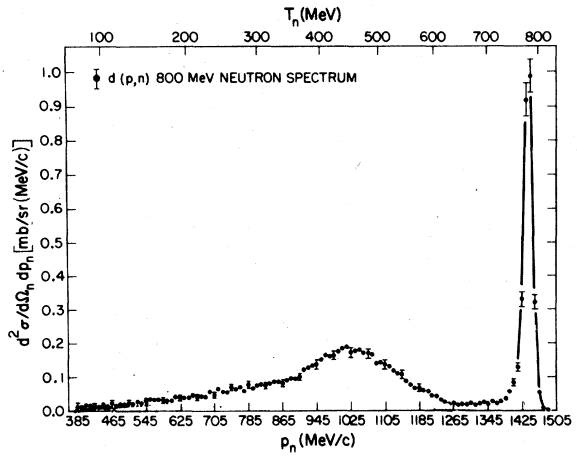

FIG. 2. 0° neutron spectrum from the reaction $pd \rightarrow nX$ at 800-MeV incident-proton energy.

The lower-energy neutrons were somewhat troublesome since they could also produce pions in the LH_2 target. Many of these undesirable pions were eliminated by means of their timing with respect to the proton-beam rf cycle, which consisted of $\frac{1}{4}$-ns-FWHM pulses every 5 ns. The "rf time" of each event, measured by the scintillation counter S_1 (Fig. 1), provided information on the incident neutron's time of flight between the LD_2 and the LH_2 targets. Unfortunately, the 5-ns beam cycle and the finite S_1 timing resolution made it impossible to distinguish 790-MeV neutrons from neutrons between $\sim$460 and 530 MeV. However, the overall effects of these lower-energy neutrons were small for the following reasons: (a) the total flux of these neutrons was about 50 percent of that in the 790-MeV peak; (b) the ratio of the pion-production cross section at 500 MeV to that at 790 MeV was estimated from the present and existing data[3–7] to be about 0.35; and (c) the upper part of the pion-energy spectrum from the 790-MeV neutrons was unavailable to pions produced from the lower-energy neutrons. Corrections applied to the data to account for pions created by the low-energy neutrons will be discussed later.

C. Spectrometer

As is shown in Fig. 1(b), the MWPC spectrometer consisted of two scintillation counters (S_1 and S_2), a bending magnet (M_2), a Čerenkov counter (C) used to tag relativistic electrons, and four wire chambers ($W_1 - W_4$). Each wire chamber contained one vertical and one horizontal set of sensing wires. The signature of a valid event was defined to be the coincidence of S_1, S_2, and at least three horizontal and three vertical MWPC signal wires. The absence of a signal from one horizontal and/or one vertical plane did not prevent the determination of a particle's momentum, since the field in the bending magnet was known as a function of position. The magnet, wire chambers, and scintillation counters S_1 and S_2 were mounted on a stand which could be pivoted about a point directly beneath the LH_2 target. This permitted measurements to be made as a function of angle. In previous experiments performed with this spectrometer,[12–14] a scintillation counter was placed upstream of the LH_2 target to veto charged beam particles. However, this counter was found to be unnecessary and in fact was a major source of the background due to charged-particle production.

The Čerenkov counter was unique to the present experiment.

The bending magnet used in the spectrometer was an H-frame magnet with "pancake" coils. The distance between pole faces was 15.2 cm (6 in.). A special current reversing switch was installed to allow the detection of both positive and negative particles. The field in the magnet was mapped at four different currents into a three-dimensional grid containing about 80 000 points. Field maps at other currents could be generated by interpolation. The overall uncertainty in the field maps was estimated to be less than 1 percent.

Each plane of the four Charpak-type multiwire chambers had 20-μm-diameter gold-plated, tungsten sense wires with a 2-mm spacing. Signals from the individual sense wires were read into combination amplifier-logic cards. A single card was capable of servicing eight adjacent wires. The first three chambers ($W_1 - W_3$) were identical, each containing 96 horizontal and 192 vertical signal wires. The last chamber (W_4) contained 192 horizontal and 320 vertical wires. The overall efficiency of each plane for detecting charged particles was typically over 99 percent.

The body of the Čerenkov counter was constructed from a 66-cm length of 25.4-cm-inside-diameter steel tubing. This tubing was used to hold isobutane gas at atmosphere pressure and was placed with its axis perpendicular to W_1 and W_2 [Fig. 1(b)]. Black polyethelyne windows, opaque to light, were located at either end of the tube. Near the back of the tube (towards W_2) a thin, elliptically shaped mirror was positioned at 45° with respect to the horizontal. Light reflected from this mirror was directed vertically through a transparent mylar window into a special light-collecting funnel.[15] This funnel, machined from Plexiglas and coated with aluminum, focused Čerenkov light onto a quartz-windowed phototube (RCA 31000Q). The Čerenkov counter was tested at the LBL 184-in. cyclotron with a 180-MeV/c negative-particle beam, with cosmic-ray muons, and with electrons and positrons at LAMPF. The detection efficiency for electrons above the 25-MeV/c threshold momentum averaged from 0.7 to 0.8. Isobutane gas was utilized in the Čerenkov counter because of its poor scintillation properties. However, knock-on electrons produced in the isobutane by a passing particle could occasionally produce enough light to trigger the phototube. The efficiency for detecting pions in this manner was found to be no greater than 0.01 during the LBL tests.

Two identical range telescopes [Fig. 1(b)] were used to detect charged particles produced by the passage of the neutron beam through a thin polyethylene radiator (N-MON) placed near the collimator exit. These telescopes provided a measure of the neutron flux for normalization purposes. A toroidal current monitor (not shown) was located in front of the LD_2 target to monitor the proton-beam current. This device gave an indication of the proton flux within about 10 percent. The condition of the LH_2 target was monitored by a range telescope (H) which detected protons scattered at 45% with respect to the incident beam line.

The spectrometer data-collection system utilized a fast intermediate buffer (called the scratch-pad memory or SPM),[16] a microprogrammed branch driver (MBD) CAMAC-computer interface,[17] and a PDP-11/20 computer. After a valid event occurred, the wire-chamber data were transferred from the MBD to the PDP-11/20 and the analog signals were sent to the MBD. During this time, the system was inhibited from accepting any more events. The system inhibition was removed once the SPM and MBD had successfully recorded the event data. The SPM wire-chamber data were subsequently sent to the PDP-11, which was capable of storing information on several events. The MBD usually transferred its contents to the PDP-11 computer during the 7.8-msec period between beam pulses but could also do this during a beam pulse if necessary. The system dead time was determined by scaling the H and N-MON counters with and without the system inhibition. A special data-handling program[18] was responsible for writing the PDP data onto magnetic tape for later off-line analysis. This program also provided an on-line analysis of the incoming events. For example, the program used the horizontal bend angle made

FIG. 3. On-line plot of particle momentum vs TOF.

by particles through the spectrometer to estimate their momenta. Figure 3 shows a typical on-line plot of particle momenta versus the time of flight (TOF) between S_1 and S_2. The pion-electron group is easily distinguished from protons and deuterons.

D. Data

Both positive and negative pions were detected with the spectrometer positioned at 10 different angles with respect to the neutron beam line (Fig. 1). These angles were 0°, 8°, 16°, 24°, 30°, 36°, 42°, 48°, 56°, and 72°. Multiple Coulomb scattering and pion decays made measurements much below 100 MeV/c impractical. Protons from elastic np collisions were detected in separate runs at all angles except 72° to determine an absolute normalization factor for the pion data. During the experiment, data were periodically obtained with the LH_2 target flask empty. This made possible the elimination of most background effects.

It was determined from a preliminary phase of this experiment that the background for negative pions was considerably more significant than the positive-pion background. Thus, more negative- than positive-pion data were collected. The difference in the background subtractions between the two types of pions can be qualitatively explained by considering the nucleons in complex nuclei (such as carbon, which was present in the LH_2 target flask) to be independent of one another. Beam neutrons, colliding with neutrons in such nuclei, can only produce negative pions, though both negative and positive pions are produced in np collisions. At 0°, where S_1 was directly in the beam, about 35% of the negative pions detected with the LH_2 target full were S_1 related and were removed by the background subtraction. In contrast, only about 15% of the positive pions were S_1 related. These percentages dropped by factors of ~ 1.5 to 3 at the larger angles where S_1 no longer directly intercepted the beam.

III. DATA ANALYSIS

A. General method

The first step in the data analysis was to determine for each event various quantities of interest, such as its momentum, polar and azimuthal scattering angles, and trajectory intersections. A Fortan computer program called TEWA (Ref. 19) converted the raw data into an array of physical quantities for each event which was stored on magnetic tape. Data output by TEWA were subsequently processed with a sorting program named KIOWA .[20] Particle identification, background subtractions, cross-section calculations, and most corrections to the data were done in KIOWA, which provided plots and histograms.

B. Single-track events

The analysis of a given event by TEWA began with the decoding of the orbit information associated with that event. This yielded the coordinates of the particle's trajectory through the wire chambers. If only one wire in each signal plane had fired (typically $\sim 80\%$ of the events), the trajectory coordinates were then entirely unambiguous. However, if two or more contiguous wires had fired in the same plane, the centroid of the hit-wire group was used as the actual coordinate. A special procedure was used to reconstruct coordinates for events lacking hit wires in one vertical and/or one horizontal plane. This procedure was based on the assumption that the incoming and outgoing trajectories should intersect near the magnet midplane. After all eight hit-wire coordinates had been determined, an initial estimate of the particle's momentum was made on the angle of deflection through the magnet. A numerical integration of the particle's path through the magnetic field was subsequently performed. By comparing the measured and calculated trajectory information, a χ^2 was determined. Minimization of this χ^2 led to small changes in the momentum and effective particle trajectory coordinates from which the final angles and momentum were determined.

C. Multiple-track events

Special treatment was required for events having more than one separate set of noncontinuous hit wires in one or more planes. If multiple groups of hit wires occurred in only one vertical and/or horizontal plane, it was possible to analyze the event by using only the coordinates in the remaining six planes and applying the reconstruction process described previously. The more complex events were analyzed by a special version of TEWA which could track all possible trajectory combinations through the magnet and determine the one with the smallest χ^2. A subset of the data was analyzed

with this program to estimate the fraction of pion events which had not been processed with the original TEWA version. For the positive-pion data, the fraction increase in the number of pions was about 0.02. The multiple hit-wire groups in this case were probably caused by δ rays and noisy wires. However, a substantial fractional increase (of up to 20%) in the number of pions was found in some of the negative-pion data taken at the smaller angles. Many of these additional events had multiple hit-wire groups in the first two chambers and a relatively large S_1 pulse height. Physically, this corresponded to the situation where the negative pion and one or both protons moved close enough together to pass through S_1, W_1, and W_2. The pulse height in S_1 was thus larger than that produced by a single pion. The bending magnet separated the particles and ultimately only the pion completed the event trigger logic (by passing through W_3, W_4, and S_2).

D. Spectrometer acceptance region

The spectrometer geometric-acceptance region was limited vertically by the magnet poles and horizontally by the wire chambers and Čerenkov counter. This region, defined in terms of the W_1 and W_2 hit-wire coordinates, did not have precise limits since particles were created at different locations in the LH_2 target. However, there was a "safe" region in which essentially all of the pions above ~ 180 MeV/c could successfully pass through the spectrometer. Below ~ 180 MeV/c the pions were deflected too drastically by multiple Coulomb scattering to travel in a predictable manner. The limits of the "safe" region were determined by the magnet current and particle momentum. Typically, this region subtended a solid angle of several msr with a 3° spread in polar scattering angle. It was necessary to adjust the magnet current two or three times at each spectrometer location to detect pions from ~ 200 MeV/c to the maximum possible momentum. The momentum bands of any two successive currents overlapped slightly to provide checks on the consistency of the measurements.

One restriction was imposed on particles satisfying the acceptance region criteria. Specifically, only events which had produced signals in at least seven wire planes were retained. Almost all of the six plane events were high-energy protons that passed through W_1 and W_2, and subsequently scattered off the frame of W_3 into W_4. This occurred more often when the negative-pion data were being collected. The rejection of six plane events caused a negligible loss of pion events.

E. Electron correction and rf selection

As mentioned previously, the mass of each particle was determined from its momentum and TOF. As a group, electrons and pions could be easily separated from the more massive particles (Fig. 3). (Here particles referred to as pions also include decay muons. The effects of these muons will be discussed shortly.) Unfortunately, electrons and pions were not separable by either mass or pulse-height information. Thus, since the Čerenkov-counter efficiency was about 0.75, some of the electrons were clearly indistinguishable from pions. As it turned out, however, this was not a problem. At spectrometer angles other than 0°, usually less than 3% of the light particles triggered the Čerenkov counter. At 0° there was a considerable electron background produced from the conversion of γ rays which were in the incident neutron beam. However, these 0° electrons could be distinguished from pions by a difference in timing with respect to the beam rf cycle. The γ rays reached the LH_2 target about 7 ns ahead of the neutrons. This provided a 2 ns difference between the electron and pion rf timing since an rf burst occurred every 5 ns. Restrictions were placed on the pion rf times not only to remove the electrons at 0°, but, as noted before, to remove the majority of pions produced by the low-energy neutrons. A systematic error of about 5% was introduced into the final cross-section results because of uncertainties associated with the positions of the rf "cuts".

F. Decay correction

It was necessary to correct the data for the finite lifetime of the pions. The fraction of pions which were able to survive the 4.9-m flight path through the spectrometer varied from ~ 0.85 at 600 MeV/c to 0.65 at 200 MeV/c. It was possible for a pion and its decay muon to satisfy collectively the spectrometer trigger logic and thus appear as a valid event. If it had been possible to identify and thus eliminate all such events (called muon events), the decay correction could have been made entirely on the known fraction of decaying pions. Unfortunately, pion and muon events were not separable

by mass or pulse-height information. Therefore, a Monte Carlo program was used to study the effects of pion decays in the spectrometer. Results from this code demonstrated that many muon events should have abnormal tracks through the spectrometer, such as large vertical bend angles and/or abnormal locations for the ingoing and outgoing track intersection. A qualitative confirmation of the code predictions was made by comparing "pion" and proton data. For nondecaying particles, deviations from a perfect track were caused mainly by multiple Coulomb scattering. Histograms of the vertical bend angle and track intersection location for pions and protons affected the same by Coulomb scattering clearly indicated the presence of abnormal events in the pion data. To remove as many muon events as possible, restrictions were placed on both the vertical bend angle and track intersection location. Appropriate limits were determined from the proton data. Over 99% of the genuine pion events were contained within these limits. The muon event contamination remaining after the cuts were applied was estimated from the Monte Carlo results to vary between about 0.02 to 0.09 as a function of momentum. These unidentifiable muon events caused slight distortions in the pion spectral shapes, since the momentum calculated by TEWA for a muon event was not always close to the momentum of the original pion. However, results from the Monte Carlo program indicated that this distortion was less than 2 percent. The preceding decay-correction method was applied directly to events having one hit wire in each plane (perfect events). As was noted before, some events required reconstruction of the hit-wire positions and thus there was not always enough information for a vertical bend angle and/or a track intersection calculation. Therefore, even though the same restrictions were placed on these nonperfect events, a smaller percentage of muon events were removed. To rectify this situation, a correction factor was applied to the nonperfect data to ensure that the same percentage of perfect and nonperfect events were removed. The decay correction introduced an error of about 5% in the pion yields at all momenta.

G. Additional corrections

The data were corrected for pion-energy losses, absorption, and elastic scattering. Pions suffered the greatest energy losses in the full LH_2 target. These losses averaged about 3 MeV at 600 MeV/c to 4 MeV at 180 MeV/c. The corrections for absorption were very small, in the neighborhood of $1-2\%$. Elastic nuclear scattering was significant only for the positive pions, where corrections up to $\sim 6\%$ were necessary to account for $\pi^+ p$ interactions in the liquid hydrogen.

It was also necessary to account for the effects of (1) the pion yields from beam neutrons between about 460 to 530 MeV, and (2) double pion production. To estimate the effects of the low-energy beam neutrons, it was assumed that all the neutrons had an energy of 500 MeV, and that the pion spectra in the colliding np c.m.s. were identical at all c.m.s. angles. The shape of the spectra was approximated by three-body Lorentz-invariant phase space integrated over all angles. The cross section ($np \rightarrow NN\pi^{\pm}$) at 500 MeV was determined to be roughly 0.7 mb from the data given in Refs. 1, 3, and 4. The resulting pion yields at 0° (laboratory) varied between 0.8 and 0.4 μb/sr MeV in the kinetic-energy interval from 90 to 210 MeV. At the larger angles, the estimated cross sections were smaller (see Table II). All the cross-section estimates were subtracted from the data. A 75% error was placed on the cross sections because of the large uncertainties involved.

Double pion production can occur around 600 MeV, and charged pions can be created in the following reactions:

$$np \rightarrow \pi^+ \pi^- np, \quad np \rightarrow \pi^+ \pi^- d,$$

$$np \rightarrow \pi^+ \pi^0 nn, \quad np \rightarrow \pi^- \pi^0 pp .$$

Very little information on these reactions below 1 GeV exists; however, it has been determined that the total cross section for the first reaction is roughly 0.5 mb at 790 MeV.[7] A pp reaction ($pp \rightarrow \pi^- \pi^+ pp$) was studied at 730 MeV.[21] The negative pions produced from this reaction were found to be concentrated at the forward angles. By using the preceding data as well as information given by Lock and Measday,[1] it was estimated that double-pion-production reactions could contribute up to $\sim 0.02-0.4$ μb/sr MeV between 100 and 150 MeV at 0° and 8° (laboratory), and less than 0.2 μb/sr MeV at the larger angles (and lower energies). No attempt was made to subtract these numbers from the data since the corrections were so poorly known. In any case, the overall effects of double pion production were probably significantly less than the effects of the 500-MeV neutrons.

H. Resolution

The spectrometer momentum resolution was mainly determined by multiple Coulomb scattering, uncertainties in the magnetic field, and variations in the amount of energy lost by pions in the liquid hydrogen. This resolution was about 10 MeV/c at all momenta. The finite width of the neutron beam further degraded the pion momentum resolution. This additional loss in resolution was estimated by calculating the maximum pion momentum kinematically possible at various laboratory angles for neutrons having energies of 781 and 799 MeV. These energies correspond to $\frac{1}{2}$ FWHM on either side of the 790-MeV neutron peak. The resulting pion momentum spread varied from about 16 MeV/c at 0° to 7 MeV/c at 72°. The overall pion momentum resolution was determined by combining the 10-MeV/c spectrometer resolution in quadrature with the resolution loss caused by the neutron beam. This overall resolution varied between $\sim$10 to 18 MeV/c, depending upon the angle. For convenience, pions were grouped into 20-MeV/c-wide bins, which is compatible with the resolution at all angles.

I. Normalization

To normalize the data, it was necessary to determine the number of 790-MeV neutrons incident on the LH_2 target for each neutron monitor count. (Only the left monitor was used, since the right monitor malfunctioned during part of the experiment.) This was done by detecting protons from the reaction $np \rightarrow np$ and comparing the proton yields to a normalized set of 790-MeV data,[22] referred to as the "N" data. In this previous experiment, a two-step process was used to obtain the "N"-data normalization. First, deuterons from the reaction $np \rightarrow \pi^0 d$ were detected as a function of angle along with protons from the elastic np reaction. The deuteron yields were subsequently compared with data on the reaction $pp \rightarrow \pi^+ d$ by means of the relation $(d\sigma/d\Omega)(np \rightarrow \pi^0 d) = \frac{1}{2}(d\sigma/d\Omega)(pp \rightarrow \pi^+ d)$. Cross-section information on the pp reaction is known to about 5%. However, the relationship between the two cross sections has an uncertainty of about 5% due to the possible breakdown of isotopic-spin invariance by Coulomb interactions. The absolute error in the normalization of the "N" data was estimated to be 7% by combining the two 5% uncertainties in quadrature. The statistical error in the number of neutrons/monitor count was far less than the 7% error in the "N"-data normalization. Thus, the overall normalization of the pion data was known to about 7%.

IV. RESULTS

A. Pion energy spectra

To provide a comparison to the results obtained by Dzhelepov *et al.*,[5] pion-kinetic-energy, rather than momentum spectra, were generated. Two types of kinetic spectra were produced—one in the laboratory coordinate system, and the other in the colliding c.m.s. Laboratory double-differential cross sections $[(d^2\sigma/d\Omega\, dT)(\bar{\theta},\bar{T})]$ and statistical errors (E) were determined at kinetic energies ($\bar{T}$) corresponding to the center of each laboratory 20-MeV/c-wide pion momentum bin. The angle $\bar{\theta}$ associated with each cross section represented an average of the angular limits of the bin. The c.m.s. cross sections $[(d^2\sigma/d\Omega^* dT^*)(\bar{\theta}^*,\bar{T}^*)]$ and statistical errors were calculated by transforming the laboratory quantities.

All the c.m.s. kinetic-energy spectra are shown in Fig. 4. The majority of the errors shown are purely statistical, though some include the uncertainty in the 500-MeV neutron correction. All the cross sections and errors displayed in these spectra are given in Tables I and II. It can be seen in Table I that the cross-section measurements associated with a given spectrum do not correspond to precisely the same c.m.s. angle. However, this was not believed to be a problem, since the spectra did not vary rapidly with a change in angle. The effective angle quoted with each spectrum represents a weighted average over all the data in that spectrum. The smooth curves drawn through many of the spectra represents a least-squares fit of the cross sections to the empirical function $F(T^*) = AT^{*5/2}(B - T^*)^2$, where A and B are adjustable coefficients that vary from spectra to spectra. The average reduced χ^2 per degree of freedom of all the fits was 1.03. The curves ($\theta^* > 57°$) serve as a guide to the eye and were used to estimate the area underneath each spectrum. Unfortunately, no satisfactory fitting function could be found for most of the spectra between 4 and 46°. The maximum pion c.m.s. kinetic energy theoretically possible from a 790-MeV neutron is 195 MeV for positive pions and 197 MeV for negative pions. However, it can be seen that the spectra often appear to reach a "cutoff" at energies slightly greater than

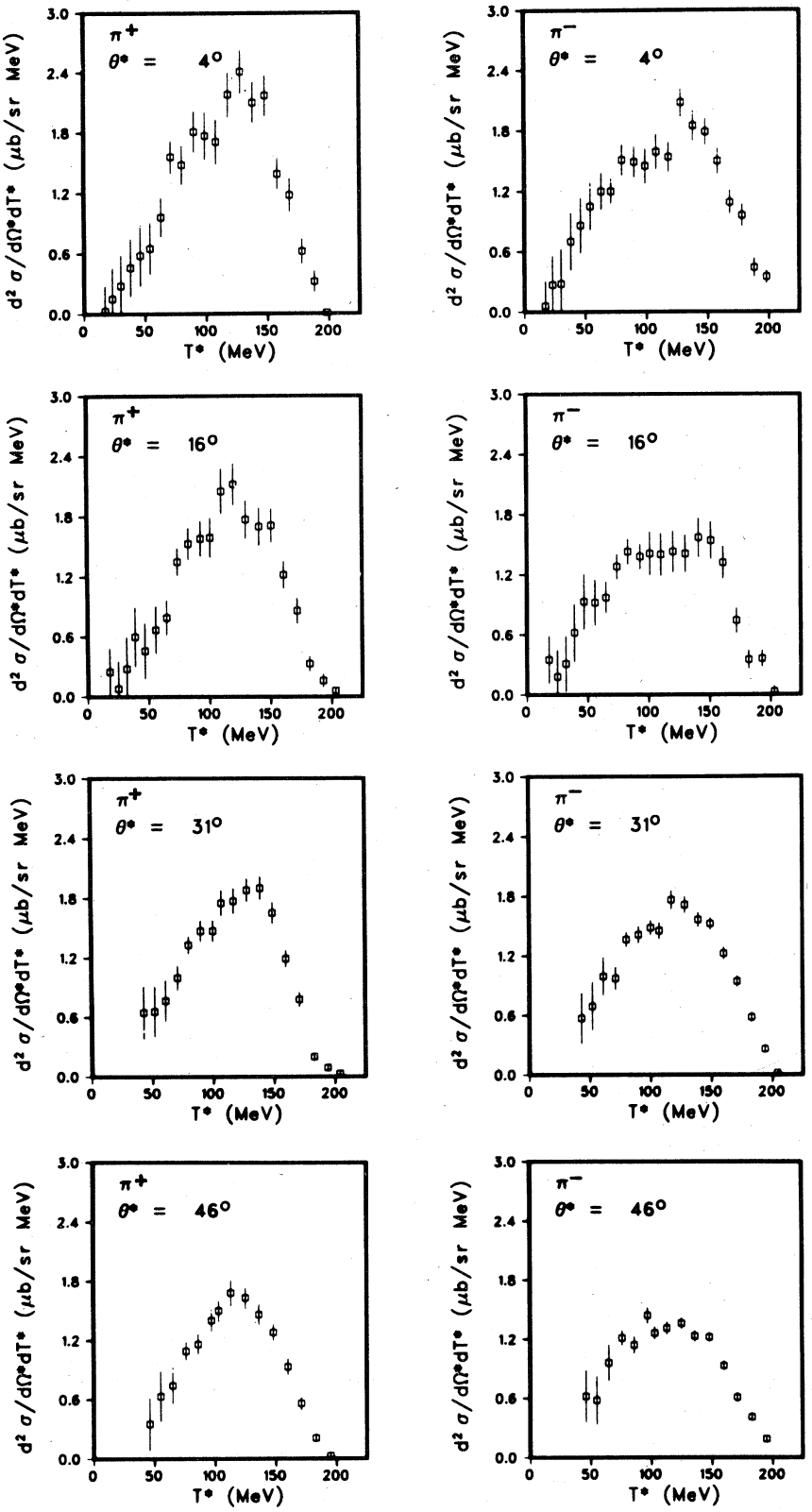

FIG. 4. Pion c.m.s. energy spectra.

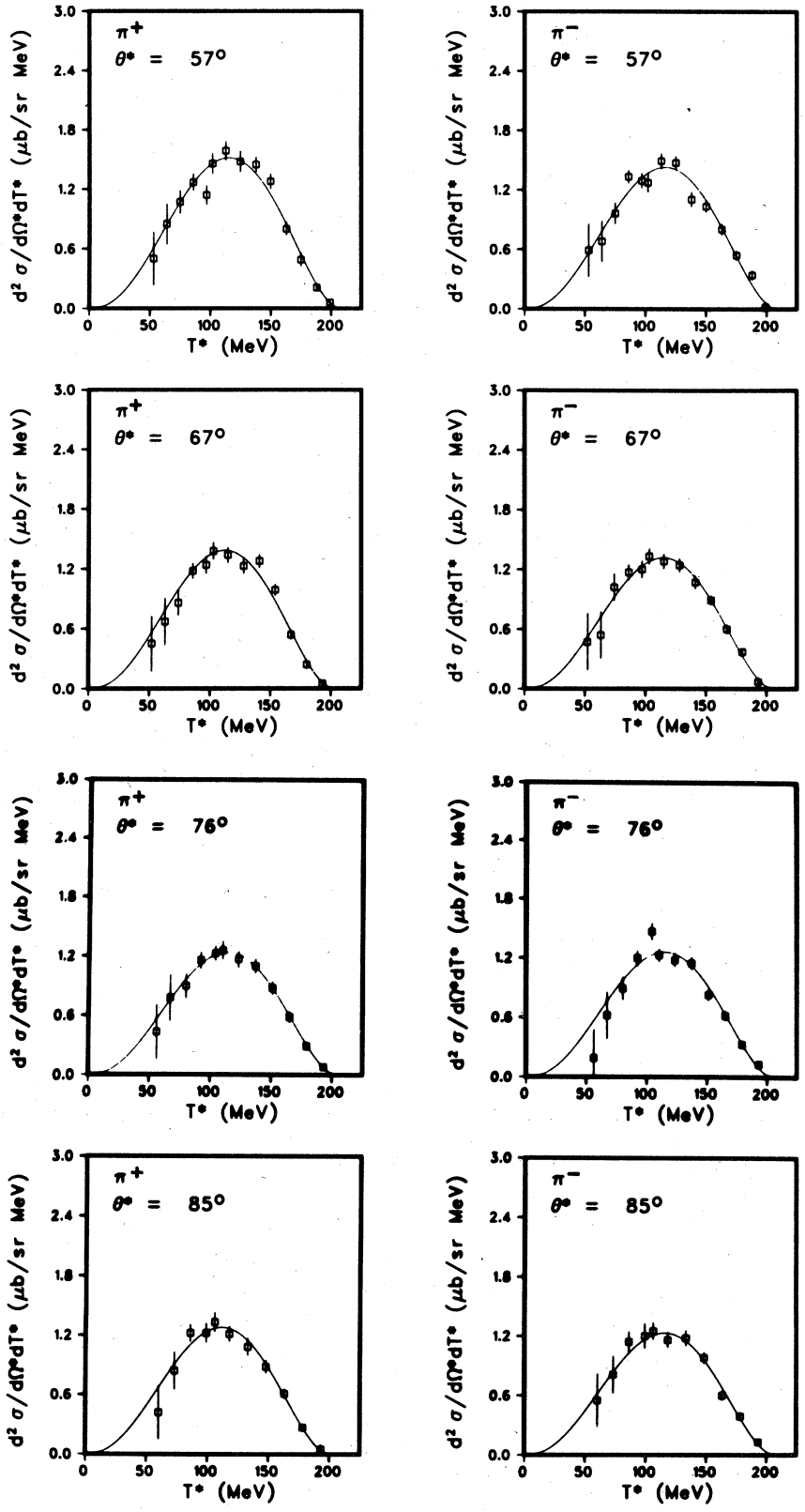

FIG. 4. *(Continued.)*

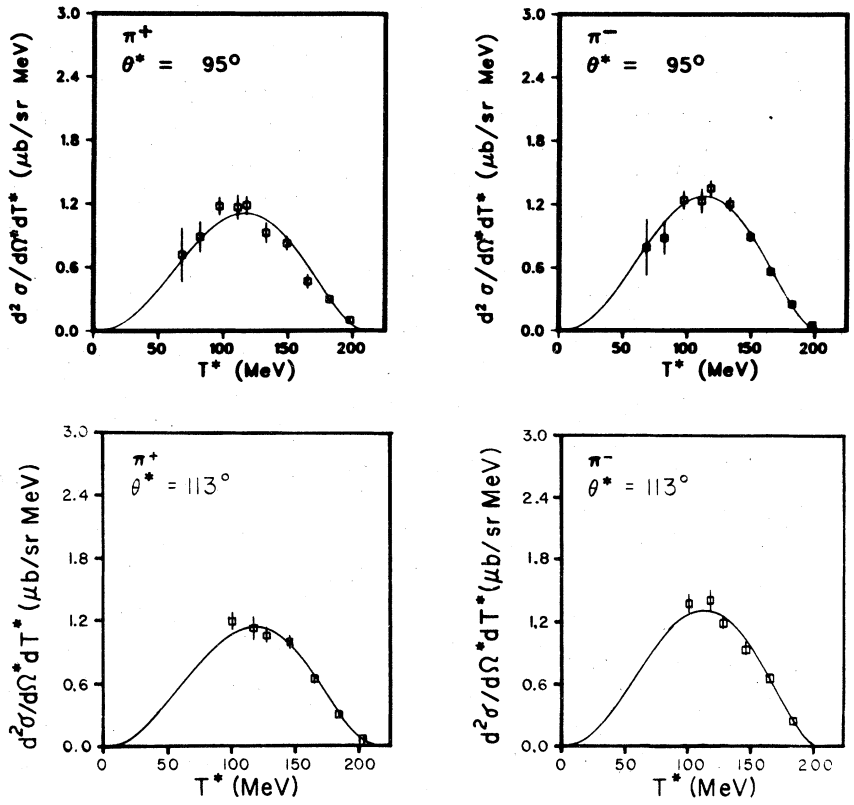

FIG. 4. *(Continued.)*

200 MeV. This was probably caused by the presence of beam neutrons having energies between 790–800 MeV as well as the finite pion-energy resolution. Nonzero cross sections were occasionally found well past 200 MeV in the raw data; however, these were believed to have been caused by muon events (momentum miscalculations by TEWA) and were therefore disregarded. It can be seen that the 4° negative-pion spectrum seems to approach the kinematic limit steeper than the other spectra. This steepness may be due to the formation of a final-state interaction of the two nucleons (protons) in this case. The lack of any indications of "peaking" in the positive-pion data may be contrary to the predictions of Phillips,[23] who concluded that the cross section for the *nn* final-state interaction should be greater than that for the the *pp* interaction.

B. Tests for differences in the π^+ and π^- spectra

At each angle, the positive- and negative-pion spectra were tested for possible asymmetries. This was done by calculating the quantity

$$R(T^*)=\frac{d^2\sigma_{\pi^+}/d\Omega^* dT^* - d^2\sigma_{\pi^-}/d\Omega^* dT^*}{(2T^*_{\max})^{-1}(d\sigma_{\pi^+}/d\Omega^* + d\sigma_{\pi^-}/d\Omega^*)}$$

which represents the difference in the double-differential cross sections divided by an "average" differential cross section. (The method used to evaluate $d\sigma_{\pi^\pm}/d\Omega^*$ will be described shortly.) The values of R versus T^* are shown in Fig. 5. The error bars represent the quadratic addition of (1) the errors given in Table I, and (2) $0.01\, d^2\sigma_{\pi^\pm}/d\Omega^* dT^*$. The latter quantities allow for fluctuations in the LH_2 target density. The regions to the right of the dashed lines in Fig. 5 contain data which were not affected by the 500-MeV neutrons. If no asymmetries were present, the data at each angle would be expected to be positioned around the line $R(T^*)=0$ with an average reduced χ^2 of ~ 1. However, when the data unaffected by the 500-MeV neutrons were fit to this line, the values of χ^2 were in some cases very large. These results are given in Table III along with the confidence level (C.L.). It is evident from this Table and Fig. 5 that asymmetries are present in the

TABLE I. Double-differential-cross-section data. All the data presented in Fig. 4 are given in this table. The cross sections denoted by the dagger have errors which were calculated as $\Delta(d^2\sigma/d\Omega\,dT)=[E^2+(\Delta C_{500})^2]^{1/2}$, $\Delta\, d^2\sigma/d\Omega^* dT^* = J\Delta\, d^2\sigma/d\Omega\,dT$, $\Delta C_{500}=500$ MeV neutron correction uncertainty ($=75\%$ of cross sections given in Table II). All the remaining cross sections are given with their statistical errors. The statistical errors given with the cross sections denoted by ‡ were increased from their original values because of possible spectrometer or beam instabilities.

$\bar{p}$ (MeV/c)	$\bar{T}$ (MeV)	$\bar{\theta}$ (deg)	$\frac{d^2\sigma_{\pi^+}}{d\Omega\,dT}$ (μb/sr MeV)	$\frac{d^2\sigma_{\pi^-}}{d\Omega\,dT}$ (μb/sr MeV)	$\bar{T}^*$ (MeV)	$\bar{\theta}^*$ (deg)	$\frac{d^2\sigma_{\pi^+}}{d\Omega^* dT^*}$ (μb/sr MeV)	$\frac{d^2\sigma_{\pi^-}}{d\Omega^* dT^*}$ (μb/sr MeV)
				Spectrometer angle=0°				
185	92	2.2	$^{\dagger}0.09^{+0.66}_{-0.09}$	$^{\dagger}0.15^{+0.66}_{-0.15}$	17	5.8	$^{\dagger}0.03^{+0.25}_{-0.03}$	$^{\dagger}0.06^{+0.25}_{-0.06}$
205	108	2.2	$^{\dagger}0.36^{+0.75}_{-0.36}$	$^{\dagger}0.66^{+0.71}_{-0.66}$	23	5.4	$^{\dagger}0.15^{+0.31}_{-0.15}$	$^{\dagger}0.27^{+0.29}_{-0.27}$
225	125	1.6	$^{\dagger}0.65^{+0.72}_{-0.65}$	$^{\dagger}0.65^{+0.81}_{-0.65}$	30	3.7	$^{\dagger}0.28^{+0.31}_{-0.28}$	$^{\dagger}0.28^{+0.35}_{-0.28}$
245	142	1.5	$^{\dagger}1.04\pm0.66$	$^{\dagger}1.56\pm0.66$	38	3.4	$^{\dagger}0.46\pm0.29$	$^{\dagger}0.70\pm0.29$
265	160	1.9	$^{\dagger}1.26\pm0.68$	$^{\dagger}1.88\pm0.60$	46	4.1	$^{\dagger}0.58\pm0.31$	$^{\dagger}0.86\pm0.28$
285	178	2.2	$^{\dagger}1.38\pm0.55$	$^{\dagger}2.23\pm0.52$	54	4.7	$^{\dagger}0.65\pm0.26$	$^{\dagger}1.05\pm0.24$
305	196	2.2	$^{\dagger}2.00\pm0.42$	$^{\dagger}2.50\pm0.40$	63	4.6	$^{\dagger}0.96\pm0.20$	$^{\dagger}1.20\pm0.19$
325	214	2.2	3.21 ± 0.35	2.48 ± 0.27	71	4.5	1.56 ± 0.17	1.20 ± 0.13
345	233	1.5	3.00 ± 0.41	3.07 ± 0.33	80	3.0	1.48 ± 0.20	1.51 ± 0.16
365	251	1.5	3.63 ± 0.43	3.00 ± 0.32	90	3.0	1.81 ± 0.21	1.49 ± 0.16
385	270	1.5	3.53 ± 0.50	2.88 ± 0.36	99	3.0	1.77 ± 0.25	1.45 ± 0.18
405	289	1.6	3.39 ± 0.45	3.15 ± 0.35	108	3.2	1.71 ± 0.23	1.59 ± 0.18
425	308	2.0	4.29 ± 0.45	3.03 ± 0.31	118	3.9	2.18 ± 0.23	1.54 ± 0.16
445	327	2.1	4.69 ± 0.44	4.07 ± 0.29	128	4.1	2.41 ± 0.23	2.08 ± 0.15
465	346	2.2	4.07 ± 0.40	3.59 ± 0.31	138	4.3	2.10 ± 0.21	1.85 ± 0.16
485	365	2.2	4.20 ± 0.42	3.45 ± 0.27	148	4.3	2.17 ± 0.21	1.79 ± 0.14
505	384	2.2	2.69 ± 0.31	2.89 ± 0.27	158	4.2	1.39 ± 0.16	1.50 ± 0.14
525	404	2.0	2.27 ± 0.32	2.10 ± 0.26	168	3.8	1.18 ± 0.17	1.09 ± 0.13
545	423	1.5	1.19 ± 0.26	1.84 ± 0.23	178	2.9	0.62 ± 0.13	0.96 ± 0.12
565	442	1.5	0.60 ± 0.22	0.84 ± 0.19	188	2.9	0.32 ± 0.11	0.44 ± 0.10
585	462	1.5	0.02 ± 0.02	0.67 ± 0.14	198	2.9	0.01 ± 0.01	0.35 ± 0.07
				Spectrometer angle=8°				
185	92	7.9	$^{\dagger}0.63\pm0.60$	$^{\dagger}0.90\pm0.60$	18	20.5	$^{\dagger}0.25\pm0.24$	$^{\dagger}0.35\pm0.24$
205	108	8.8	$^{\dagger}0.18^{+0.67}_{-0.18}$	$^{\dagger}0.42^{+0.64}_{-0.42}$	25	21.3	$^{\dagger}0.08^{+0.28}_{-0.08}$	$^{\dagger}0.18^{+0.27}_{-0.18}$
225	125	9.4	$^{\dagger}0.64^{+0.72}_{-0.64}$	$^{\dagger}0.69\pm0.64$	32	21.6	$^{\dagger}0.28^{+0.32}_{-0.28}$	$^{\dagger}0.31\pm0.28$
245	142	6.7	$^{\dagger}1.32\pm0.67$	$^{\dagger}1.36\pm0.63$	39	14.9	$^{\dagger}0.60\pm0.30$	$^{\dagger}0.62\pm0.29$
265	160	7.2	$^{\dagger}0.98\pm0.60$	$^{\dagger}1.99\pm0.59$	47	15.6	$^{\dagger}0.46\pm0.28$	$^{\dagger}0.93\pm0.28$

TABLE I. *(Continued.)*

$\bar{p}$ (MeV/c)	$\bar{T}$ (MeV)	$\bar{\theta}$ (deg)	$\frac{d^2\sigma_{\pi^+}}{d\Omega\, dT}$ (μb/sr MeV)	$\frac{d^2\sigma_{\pi^-}}{d\Omega\, dT}$ (μb/sr MeV)	$\bar{T}^*$ (MeV)	$\bar{\theta}^*$ (deg)	$\frac{d^2\sigma_{\pi^+}}{d\Omega^* dT^*}$ (μb/sr MeV)	$\frac{d^2\sigma_{\pi^-}}{d\Omega^* dT^*}$ (μb/sr MeV)
				Spectrometer angle = 8°				
285	178	8.0	†1.41±0.50	†1.93±0.48	56	16.9	†0.67±0.24	†0.92±0.23
305	196	8.6	†1.62±0.36	†1.99±0.33	65	17.8	†0.79±0.18	†0.97±0.16
325	214	9.1	2.71±0.29	2.58±0.25	74	18.6	1.35±0.14	1.28±0.13
345	233	9.4	3.03±0.33	2.84±0.27	83	18.9	1.53±0.16	1.43±0.13
365	251	9.4	3.11±0.35	2.71±0.25	93	18.7	1.58±0.18	1.38±0.13
385	270	6.7	3.13±0.39	‡2.77±0.43	101	13.3	1.59±0.20	‡1.41±0.22
405	289	6.8	4.01±0.45	‡2.73±0.43	110	13.4	2.05±0.23	‡1.40±0.22
425	308	7.4	4.11±0.41	‡2.77±0.40	120	14.5	2.12±0.21	‡1.43±0.21
445	327	7.8	3.40±0.36	‡2.72±0.37	130	15.2	1.77±0.19	‡1.41±0.19
465	346	8.3	3.25±0.36	‡3.00±0.38	141	16.0	1.70±0.19	‡1.57±0.20
485	365	8.6	3.26±0.32	‡2.93±0.37	151	16.5	1.71±0.17	‡1.54±0.19
505	384	9.0	2.31±0.27	‡2.50±0.33	161	17.2	1.22±0.14	‡1.32±0.17
525	404	9.2	1.63±0.25	‡1.40±0.24	172	17.6	0.86±0.13	‡0.74±0.13
545	423	9.4	0.63±0.16	‡0.65±0.19	182	17.9	0.33±0.08	‡0.35±0.10
565	442	9.4	0.29±0.13	‡0.68±0.16	193	17.8	0.16±0.07	‡0.36±0.09
585	462	9.4	0.11±0.07	$\ddagger 0.06^{+0.11}_{-0.06}$	203	17.8	0.06±0.03	$\ddagger 0.03^{+0.06}_{-0.03}$
				Spectrometer angle = 16°				
245	142	14.7	†1.35±0.57	†1.19±0.55	43	32.0	†0.65±0.27	†0.57±0.26
265	160	15.2	†1.33±0.52	†1.41±0.51	52	32.2	†0.66±0.26	†0.69±0.25
285	178	16.0	†1.52±0.41	†1.96±0.40	61	33.1	†0.77±0.21	†0.99±0.20
305	196	16.6	†1.95±0.25	†1.89±0.24	71	33.7	†1.00±0.13	†0.97±0.12
325	214	17.0	2.55±0.18	2.60±0.16	80	34.0	1.33±0.09	1.36±0.08
345	233	17.4	2.77±0.21	2.65±0.17	90	34.3	1.47±0.11	1.41±0.09
365	251	17.4	2.76±0.20	2.78±0.15	100	34.0	1.47±0.11	1.48±0.08
385	270	14.7	3.31±0.25	2.74±0.18	107	28.7	1.75±0.13	1.45±0.09
405	289	14.8	3.34±0.25	3.32±0.19	117	28.7	1.77±0.13	1.76±0.10
425	308	15.4	3.51±0.23	3.18±0.16	128	29.7	1.88±0.12	1.71±0.09
445	327	15.8	3.51±0.22	2.89±0.15	139	30.2	1.90±0.12	1.56±0.08
465	346	16.2	3.03±0.19	2.79±0.14	149	30.8	1.65±0.11	1.52±0.07
485	365	16.6	2.18±0.17	2.22±0.12	160	31.4	1.19±0.09	1.22±0.07

TABLE I. *(Continued.)*

$\bar{p}$ (MeV/c)	$\bar{T}$ (MeV)	$\bar{\theta}$ (deg)	$\frac{d^2\sigma_{\pi^+}}{d\Omega\, dT}$ (μb/sr MeV)	$\frac{d^2\sigma_{\pi^-}}{d\Omega\, dT}$ (μb/sr MeV)	$\bar{T}^*$ (MeV)	$\bar{\theta}^*$ (deg)	$\frac{d^2\sigma_{\pi^-}}{d\Omega^* dT^*}$ (μb/sr MeV)	$\frac{d^2\sigma_{\pi^-}}{d\Omega^* dT^*}$ (μb/sr MeV)
				Spectrometer angle=16°				
505	384	16.9	1.42±0.14	1.71±0.10	171	31.9	0.78±0.08	0.94±0.06
525	404	17.2	0.36±0.08	1.05±0.09	183	32.3	0.20±0.04	0.58±0.05
545	423	17.4	0.16±0.06	0.47±0.07	194	32.6	0.09±0.03	0.26±0.04
565	442	17.4	0.06±0.03	$0.03^{+0.04}_{-0.03}$	204	32.5	0.03±0.02	0.02±0.02
				Spectrometer angle=24°				
235	134	22.8	†0.68±0.52	†1.20±0.52	46	48.4	†0.35±0.27	†0.62±0.27
255	151	23.5	†1.19±0.48	†1.09±0.47	55	48.4	†0.63±0.26	†0.58±0.25
275	169	24.2	†1.35±0.34	†1.76±0.34	65	48.7	†0.74±0.19	†0.96±0.19
295	187	24.8	1.96±0.17	2.17±0.14	76	49.0	1.09±0.10	1.21±0.08
315	205	25.3	2.06±0.20	2.01±0.16	86	49.3	1.16±0.11	1.14±0.09
335	223	25.4	2.45±0.21	2.52±0.17	97	48.9	1.40±0.12	1.44±0.09
355	242	22.7	2.68±0.22	2.25±0.13	103	43.8	1.50±0.12	1.26±0.07
375	261	22.8	3.00±0.25	2.34±0.13	113	43.6	1.68±0.14	1.31±0.07
395	279	23.4	2.88±0.22	2.40±0.10	125	44.4	1.63±0.12	1.36±0.06
415	298	23.9	2.55±0.19	2.14±0.10	136	45.0	1.46±0.11	1.23±0.06
435	317	24.4	2.21±0.16	2.11±0.09	148	45.6	1.28±0.09	1.22±0.05
455	336	24.8	1.59±0.15	1.61±0.08	160	46.1	0.93±0.09	0.93±0.05
475	356	25.0	0.95±0.11	1.04±0.07	171	46.3	0.56±0.07	0.61±0.04
495	375	25.4	0.35±0.07	0.69±0.06	183	46.8	0.21±0.04	0.41±0.04
515	394	25.4	$0.04^{+0.05}_{-0.04}$	0.32±0.05	195	46.7	0.03±0.03	0.19±0.03
				Spectrometer angle=30°				
235	134	29.2	†0.88±0.48	†1.04±0.47	53	59.6	†0.50±0.27	†0.59±0.27
255	151	30.0	†1.46±0.36	†1.18±0.36	64	59.7	†0.85±0.21	†0.68±0.21
275	169	30.7	†1.81±0.21	†1.63±0.19	75	59.8	†1.07±0.12	†0.96±0.11
295	187	31.2	2.11±0.15	2.23±0.12	86	59.8	1.27±0.09	1.33±0.07
315	205	31.4	1.88±0.16	2.14±0.13	97	59.4	1.14±0.10	1.29±0.08
335	223	28.7	2.48±0.19	2.16±0.17	102	54.5	1.46±0.11	1.27±0.10
355	242	28.8	2.67±0.17	2.50±0.14	113	54.2	1.59±0.10	1.49±0.08
375	261	29.4	2.46±0.19	2.44±0.12	125	54.8	1.48±0.11	1.47±0.07

TABLE I *(Continued.)*

$\bar{p}$ (MeV/c)	$\bar{T}$ (MeV)	$\bar{\theta}$ (deg)	$\frac{d^2\sigma_{\pi^+}}{d\Omega dT}$ (μb/sr MeV)	$\frac{d^2\sigma_{\pi^-}}{d\Omega dT}$ (μb/sr MeV)	$\bar{T}^*$ (MeV)	$\bar{\theta}^*$ (deg)	$\frac{d^2\sigma_{\pi^+}}{d\Omega^* dT^*}$ (μb/sr MeV)	$\frac{d^2\sigma_{\pi^-}}{d\Omega^* dT^*}$ (μb/sr MeV)
				Spectrometer angle=30°				
395	279	30.0	2.38±0.13	1.81±0.13	138	55.5	1.45±0.08	1.10±0.08
415	298	30.4	2.09±0.13	1.69±0.10	150	55.8	1.28±0.08	1.03±0.06
435	317	30.8	1.29±0.11	1.29±0.09	163	56.2	0.80±0.07	0.80±0.06
455	336	31.2	0.79±0.11	0.88±0.08	175	56.6	0.49±0.07	0.54±0.05
475	356	31.4	0.33±0.06	0.54±0.08	188	56.8	0.21±0.04	0.34±0.05
495	375	31.4	0.09±0.03	$0.03^{+0.08}_{-0.03}$	199	56.6	0.06±0.02	$0.02^{+0.05}_{-0.02}$
				Spectrometer angle=36°				
215	117	35.0	†0.74±0.46	†0.78±0.47	52	70.5	†0.45±0.28	†0.47±0.29
235	134	35.9	†1.07±0.39	†0.87±0.39	63	70.2	†0.67±0.24	†0.54±0.24
255	151	36.6	†1.36±0.21	†1.60±0.22	74	70.0	†0.86±0.13	†1.02±0.14
275	169	37.2	1.83±0.12	1.82±0.12	86	69.8	1.18±0.08	1.17±0.08
295	187	37.4	1.91±0.14	1.85±0.13	97	69.3	1.24±0.09	1.20±0.09
315	205	34.7	2.19±0.14	2.12±0.13	103	64.6	1.38±0.09	1.33±0.08
335	223	34.8	2.11±0.13	2.02±0.13	115	64.2	1.34±0.08	1.28±0.08
355	242	35.6	1.92±0.13	1.93±0.11	128	64.9	1.23±0.08	1.24±0.07
375	261	36.0	1.97±0.11	1.65±0.10	141	65.2	1.28±0.07	1.07±0.07
395	279	36.5	1.51±0.10	1.37±0.08	154	65.6	0.99±0.06	0.89±0.05
415	298	36.9	0.82±0.08	0.92±0.08	167	65.9	0.54±0.05	0.60±0.05
435	317	37.3	0.37±0.06	0.56±0.06	180	66.2	0.24±0.04	0.37±0.04
455	336	37.4	0.08±0.02	0.10±0.06	193	66.2	0.05±0.02	0.07±0.04
				Spectrometer angle=42°				
205	108	41.0	†0.65±0.42	†0.28±0.43	56	80.1	†0.43±0.28	†0.19±0.29
225	125	41.8	†1.13±0.35	†0.92±0.35	67	79.4	†0.77±0.24	†0.62±0.24
245	142	42.6	†1.29±0.19	†1.29±0.18	80	79.1	†0.89±0.13	†0.89±0.12
265	160	43.2	1.65±0.13	1.71±0.12	92	78.8	1.15±0.09	1.20±0.08
285	178	43.4	1.73±0.12	2.10±0.12	104	78.2	1.22±0.08	1.47±0.09
305	196	40.7	1.84±0.14	1.81±0.11	110	73.7	1.25±0.10	1.23±0.07
325	214	41.0	1.70±0.13	1.72±0.10	123	73.6	1.16±0.09	1.18±0.07
345	233	41.6	1.57±0.11	1.66±0.10	137	73.9	1.09±0.08	1.15±0.07
365	251	42.2	1.25±0.10	1.19±0.08	151	74.3	0.87±0.07	0.83±0.06
385	270	42.7	0.82±0.08	0.88±0.07	165	74.7	0.58±0.06	0.62±0.05
405	289	43.0	0.40±0.06	0.47±0.05	179	74.8	0.29±0.04	0.33±0.04
425	308	43.4	0.11±0.03	0.19±0.04	193	75.1	0.08±0.02	0.13±0.03

TABLE I. *(Continued.)*

$\bar{p}$ (MeV/c)	$\bar{T}$ (MeV)	$\bar{\theta}$ (deg)	$\frac{d^2\sigma_{\pi^+}}{d\Omega\, dt}$ (μb/sr MeV)	$\frac{d^2\sigma_{\pi^-}}{d\Omega\, dT}$ (μb/sr MeV)	$\bar{T}^*$ (MeV)	$\bar{\theta}^*$ (deg)	$\frac{d^2\sigma_{\pi^+}}{d\Omega^* dT^*}$ (μb/sr MeV)	$\frac{d^2\sigma_{\pi^-}}{d\Omega^* dT^*}$ (μb/sr MeV)
				Spectrometer angle=48°				
195	100	47.3	†0.57±0.37	†0.75±0.37	60	89.2	†0.42±0.27	†0.55±0.27
215	117	48.3	†1.12±0.26	†1.09±0.26	73	88.5	†0.84±0.19	†0.81±0.19
235	134	49.0	1.61±0.12	1.51±0.15	86	87.9	1.22±0.09	1.14±0.11
255	151	49.4	1.61±0.13	1.58±0.17	99	87.3	1.22±0.10	1.20±0.13
275	169	46.7	1.81±0.14	1.70±0.12	106	83.0	1.33±0.10	1.25±0.09
295	187	46.8	1.65±0.11	1.57±0.11	118	82.3	1.21±0.08	1.16±0.08
315	205	47.6	1.45±0.12	1.58±0.11	133	82.7	1.08±0.09	1.18±0.08
335	223	48.2	1.18±0.09	1.30±0.08	148	83.0	0.88±0.07	0.98±0.06
355	242	48.7	0.81±0.07	0.80±0.07	163	83.2	0.61±0.05	0.60±0.05
375	261	49.1	0.36±0.05	0.51±0.06	178	83.3	0.27±0.04	0.39±0.04
395	279	49.4	0.07±0.07	0.16±0.04	193	83.4	0.05±0.05	0.13±0.03
				Spectrometer angle=56°				
185	92	55.3	†0.87±0.31	†0.95±0.32	68	99.3	†0.72±0.26	†0.79±0.27
205	108	56.4	†1.06±0.18	†1.05±0.19	82	98.6	†0.89±0.15	†0.88±0.16
225	125	57.1	1.39±0.11	1.46±0.11	97	97.9	1.18±0.09	1.24±0.09
245	142	57.4	1.38±0.14	1.45±0.14	111	97.1	1.17±0.12	1.23±0.12
265	160	54.7	1.46±0.11	1.65±0.10	118	93.1	1.19±0.09	1.35±0.08
285	178	55.1	1.13±0.12	1.47±0.08	133	92.8	0.93±0.10	1.20±0.07
305	196	55.8	1.01±0.08	1.07±0.07	149	93.0	0.83±0.07	0.89±0.05
325	214	56.4	0.56±0.08	0.67±0.05	165	93.2	0.47±0.07	0.56±0.04
345	233	56.9	0.36±0.05	0.29±0.04	182	93.3	0.30±0.04	0.25±0.04
365	251	57.3	0.12±0.03	0.05±0.03	198	93.4	0.10±0.02	0.05±0.03
				Spectrometer angle=72°				
185	92	72.7	1.14±0.09	1.30±0.09	101	115.6	1.20±0.10	1.38±0.10
205	108	73.3	1.07±0.11	1.34±0.10	118	114.8	1.13±0.12	1.41±0.11
225	125	70.7	1.04±0.08	1.18±0.07	128	111.4	1.06±0.08	1.19±0.07
245	142	71.4	0.99±0.07	0.92±0.07	146	111.1	1.00±0.07	0.94±0.07
265	160	72.1	0.64±0.05	0.65±0.05	165	111.1	0.65±0.05	0.66±0.05
285	178	72.8	0.29±0.03	0.25±0.03	184	111.2	0.30±0.03	0.25±0.03
305	196	73.2	0.07±0.02		203	111.1	0.07±0.02	

TABLE II. 500-MeV neutron correction. This table lists all the double-differential cross sections ($d^2\sigma/d\Omega\, dT_{500}$) which were subtracted from the data.

$\bar{p}$ (MeV/c)	$\bar{T}$ (MeV)	$\frac{d^2\sigma}{d\Omega\, dT_{500}}$ (μb/sr MeV)	$\bar{p}$ (MeV)/c)	$\bar{T}$ (MeV)	$\frac{d^2\sigma}{d\Omega\, dT_{500}}$ (μb/sr MeV)
Spectrometer angle=0°			Spectrometer angle=8°		
185	92	0.75	185	92	0.70
205	108	0.80	205	108	0.75
225	125	0.80	225	125	0.75
245	142	0.75	245	142	0.75
265	160	0.70	265	160	0.70
285	178	0.60	285	178	0.55
305	196	0.40	305	196	0.30
Spectrometer angle=16°			Spectrometer angle=24°		
245	142	0.70	235	134	0.65
265	160	0.65	255	151	0.60
285	178	0.50	275	169	0.40
305	196	0.25			
Spectrometer angle=30°			Spectrometer angle=36°		
235	134	0.60	215	117	0.60
255	151	0.45	235	134	0.50
275	169	0.20	255	151	0.25
Spectrometer angle=42°			Spectrometer angle=48°		
205	108	0.55	195	100	0.45
225	125	0.45	215	117	0.30
245	142	0.20			
Spectrometer angle=56°			Spectrometer angle=72°		
185	92	0.40	no corrections made		
205	108	0.20			

data. In most of the spectra from 4—85°, the negative-pion yields are predominant in the region from about 160 to 200 MeV. On the other hand, the positive pions are predominant below about 160 MeV. This pattern appears to be reversed in the spectra at 95 and 113°. It is difficult to explain the size of the asymmetries (often $>10\%$) solely from charge and mass differences between the final states $pp\pi^-$ and $nn\pi^+$.[23] Thus it seems possible that interfering $T=0$ and $T=1$ amplitudes are causing at least some of the asymmetry.

C. Pion differential and total cross sections

To determine the differential cross section $d\sigma/d\Omega^*$ at each angle it was necessary to integrate each spectrum over all possible kinetic energies. This was done by combining the area underneath the data points with an estimate of the "missing" area. The region containing the data points (N in number) was integrated by dividing it up into a set of intervals (ΔT_j^*). Each interval contained one cross section. The limits of all but two of the intervals were defined by the kinetic-energy midpoint between adjacent measurements. The first and last intervals (corresponding to the cross sections at the lowest and highest energies) had a length which represented the distance between the cross section and its nearest neighbor. The area underneath the data points (S) was thus given by

$$\sum_{j=1}^{N} \frac{d^2\sigma_j}{d\Omega^* dT^*} \Delta T_j \ .$$

An error associated with S (ΔS) was determined by combining in quadrature the individual products of

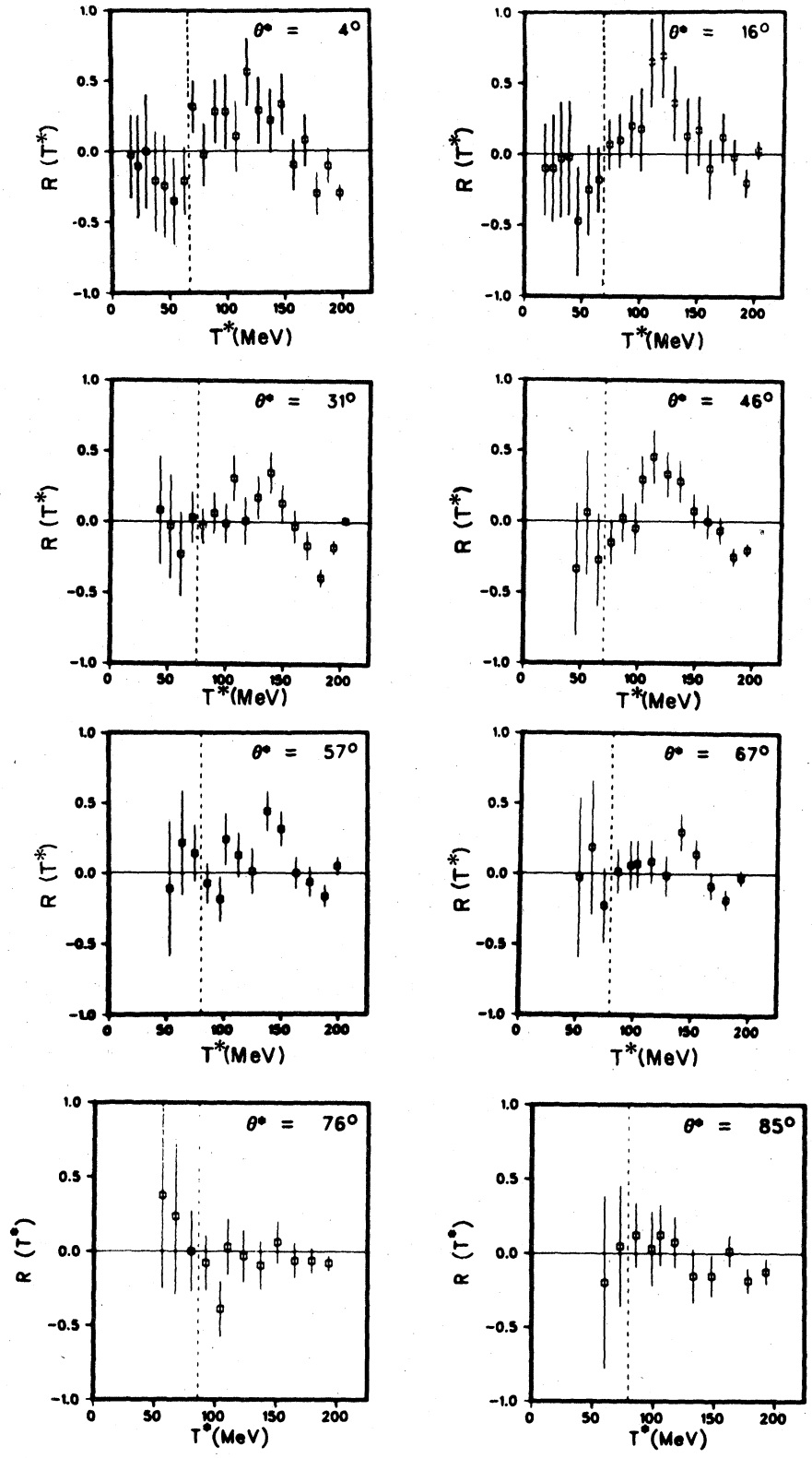

FIG. 5. R versus T^*.

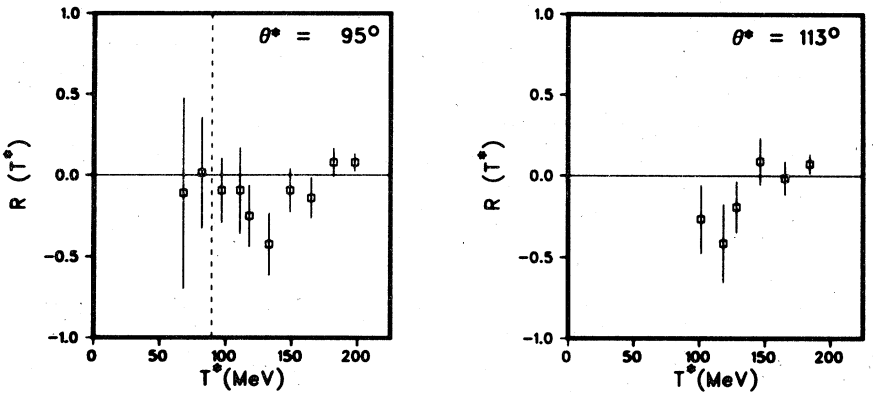

FIG. 5. *(Continued).*

the cross-section errors given in Table I and the interval widths ΔT_j. The area underneath the missing portion of each spectrum fitted to the empirical curve (I) was estimated by simply integrating the curve over the appropriate region. An error of 50% was assigned to I, based on comparisons to areas underneath other possible extrapolations. The missing area in each of the remaining spectra (I') was estimated by connecting the points (0,0) and $(\overline{T}_{j=1,3}, \overline{d\sigma}_{j=1,3}/d\Omega^* dT^*)$ with a straight line. The latter quantity represents an average over the three data points gathered at the lowest energies. An error of 50% was assigned to I'. The differential cross section at each angle was given by $S+I$ or $S+I'$. All the values of $d\sigma/d\Omega^*$ are listed in Table IV, along with S, ΔS, I, or I', and an overall error $\Delta\, d\sigma/d\Omega^*$. This error consisted of three separate errors combined in quadrature—ΔS, $0.5I$ or $0.5I'$, and $0.01\, d\sigma/d\Omega^*$. The last error was included to allow for possible LH_2 target density variations. Additional errors, such as those inherent in the decay correction and "rf cuts," were not included.

TABLE III. Summary of the tests for differences between the positive- and negative-pion spectra.

θ^*(deg)	χ^2	C.L.
4	3.08	0.000 08
16	1.24	0.24
31	4.66	0.000 000 01
46	3.66	0.000 02
57	2.20	0.012
67	1.27	0.24
76	0.84	0.58
85	1.01	0.43
95	1.41	0.19
113	2.85	0.006

The angular variation of $d\sigma/d\Omega^*$ can be expressed as follows:

$$\frac{d\sigma_{\pi^\pm}}{d\Omega^*}(\theta^*)=\sum a_n^{\pi^\pm}\cos^n(\theta^*),\quad n=0,1,2,\cdots . \tag{4}$$

Charge symmetry requires that $a_n^{\pi^+}=a_n^{\pi^-}$ for even n, and $a_n^{\pi^+}=-a_n^{\pi^-}$ for odd n. By forming the quantities given below, it is possible to calculate separately the coefficients with even and odd indices:

$$\frac{1}{2}\left[\frac{d\sigma_{\pi^+}}{d\Omega^*}(\theta^*)+\frac{d\sigma_{\pi^-}}{d\Omega^*}\right]=\sum a_{2n}\cos^{2n}(\theta^*)\,, \tag{5}$$

$$\frac{1}{2}\left[\frac{d\sigma_{\pi^+}}{d\Omega^*}(\theta^*)-\frac{d\sigma_{\pi^-}}{d\Omega^*}(\theta^*)\right]=\sum a_{2n+1}\cos^{2n+1}(\theta^*)\,. \tag{6}$$

$$n=0,1,2,\ a_{2n}=a_{2n}^{\pi^+}=a_{2n}^{\pi^-}\,,$$

A complete angular distribution of positive (negative) pions from $\sim 0°$ to 180° can be obtained by reflecting the negative- (positive-) pion data about 90° if we use the assumption of charge symmetry. The first case is symbolized in Eq. (7):

$$\frac{d\sigma_{\pi^+}}{d\Omega^*}(\theta^*),\ \frac{d\sigma_{\pi^-}}{d\Omega^*}(180°-\theta^*) =\sum a_n\cos^n(\theta^*),\quad a_n=a_n^{\pi^+}\,. \tag{7}$$

The computer program CURFIT[24] was used to fit the data to Eqs. (4)—(7). Errors on the sums and differences of $d\sigma_{\pi^\pm}/d\Omega^*$ as used in Eqs. (5) and

TABLE IV. Differential-cross-section results (all quantities except θ^* in μb/sr).

θ^* (deg)	$\frac{d\sigma_{\pi^+}}{d\Omega^*}$	S_{π^+}	I_{π^+} (or I_{π^+}')
4	226±9	226±9	<0.5
16	202±8	202±8	<0.5
31	190±6	185±5	5
46	158±6	154±5	4
57	160±7	152±5	8
67	139±6	132±5	7
76	126±7	118±5	8
85	127±7	117±5	10
95	119±8	107±5	12
113	125±19	88±3	37
θ^* (deg)	$\frac{d\sigma_{\pi^-}}{d\Omega^*}$	S_{π^-}	I_{π^-} (or I_{π^-}')
4	219±8	219±8	<0.5
16	190±8	189±8	1
31	190±6	185±5	5
46	158±6	152±5	6
57	150±6	143±5	7
67	136±6	130±5	6
76	127±7	119±5	8
85	130±7	121±5	9
95	131±9	117±5	14
113	138±22	94±3	44

(6) were calculated by combining the errors $\Delta d\sigma_{\pi^\pm}/d\Omega^*$ in quadrature. Figures 6 and 7 show the best fits to Eqs. (6) and (7). In the latter case, the cross sections at 67, 85, 95, and 113° were determined by averaging the four sets of cross sections $[(d\sigma_{\pi^+}/d\Omega^*)(67°),(d\sigma_{\pi^-}/d\Omega^*)(113°)]$, $[(d\sigma_{\pi^+}/d\Omega^*)(85°),(d\sigma_{\pi^-}/d\Omega^*)(95°)]$, $[(d\sigma_{\pi^+}/d\Omega^*)(95°),(d\sigma_{\pi^-}/d\Omega^*)(85°)]$, and

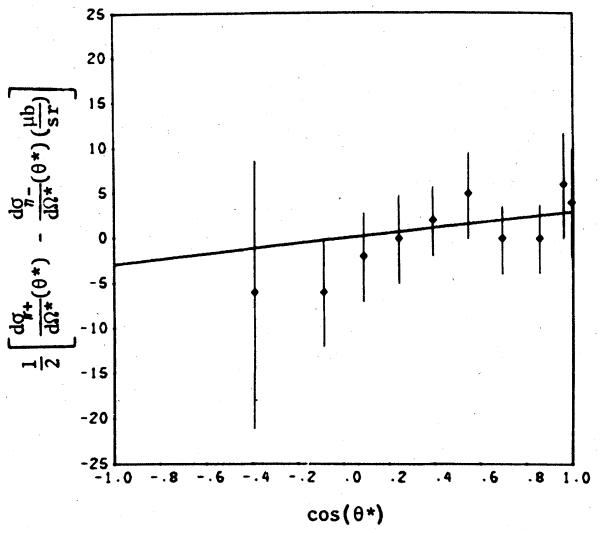

FIG. 6. The subtraction of $d\sigma_{\pi^-}/d\Omega^*$ from $d\sigma_{\pi^+}/d\Omega^*$. The straight line represents the function $d\sigma/d\Omega^*=2.9\cos(\theta^*)\mu$b/sr.

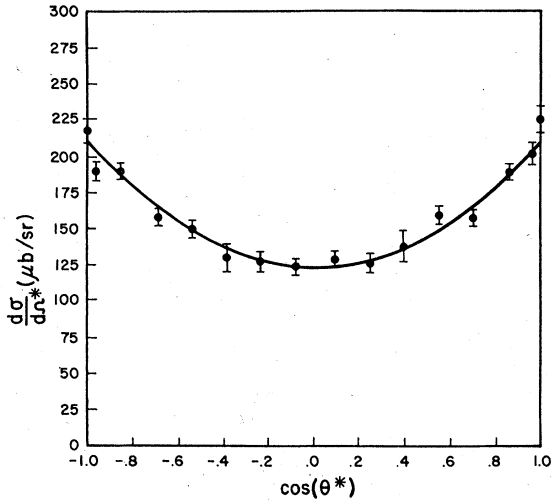

FIG. 7. Complete pion angular distribution. The curve represents the best estimate of $d\sigma/d\Omega^*$.

TABLE V. A summary of the coefficients of polynomials fitted to $(d\sigma_{\pi^+}/d\Omega^*)(\theta^*)$, $(d\sigma_{\pi^-}/d\Omega^*)(\theta^*)$, etc. (all coefficients in μb/sr).

Equation No.				χ^2
(4) (π^+)	$a_0=122.7\pm3.4$	$a_2=92.0\pm6.8$		0.97
(4) (π^-)	$a_0=124.9\pm3.5$	$a_2=83.0\pm6.6$		0.87
(7)	$a_0=123.1\pm2.7$	$a_2=88.3\pm4.9$		1.04
(5)	$a_0=123.7\pm2.4$	$a_2=87.6\pm4.7$		1.48
(5)	$a_0=126.0\pm3.0$	$a_2=65.3\pm17.7$	$a_4=23.9\pm18.3$	1.45
(7)	$a_0=125.1\pm3.2$	$a_2=68.7\pm17.9$	$a_4=20.9\pm18.4$	1.02
(7)	$a_0=123.1\pm2.7$	$a_1=2.7\pm2.6$	$a_2=88.3\pm4.9$	1.04
(6)	$a_1=2.9\pm2.5$			0.30
(6)	$a_3=3.6\pm3.5$			0.32

$[(d\sigma_{\pi^+}/d\Omega^*)(113°),(d\sigma_{\pi^-}/d\Omega^*)(67°)]$. It can be seen from Table V that $d\sigma/d\Omega^*$ was probably best represented by the polynomial $a_0+a_2\cos^2(\theta^*)$. It was impossible to determine conclusively if any odd powers of $\cos(\theta^*)$ were present, since the differences between $d\sigma_{\pi^\pm}/d\Omega^*$ were small compared to the errors involved. The best estimate of $(d\sigma/d\Omega^*)(\theta^*)$ was taken to be $(123.1\pm2.7)+(88.3\pm4.9)\cos^2(\theta^*)]$ μb/sr as determined from Eq. (7). This distribution was chosen since it gave an excellent fit to 16 data points with only two coefficients.

The total cross section, obtained by integrating the "best estimate" of $d\sigma/d\Omega^*$, was 1.92 mb. The absolute error on this number was determined to be 0.20 mb by combining errors introduced by the rf cuts, decay correction, and normalization together with the uncertainty present in the fitted parameters a_0 and a_2.

D. Estimates of $d\sigma_{01}/d\Omega^*$ and σ_{01}

It was mentioned earlier that the cross section σ_{01} is given by $2\sigma(np\to NN\pi^\pm)-\sigma_{11}$, where σ_{11} is just $\sigma(pp\to pp\pi^0)$. No experiments have been performed to determine the value of σ_{11} at 790 MeV. However, there are measurements at 735, 925, and 970 MeV.[25–27] The cross section σ_{11} at 790 MeV was estimated to be 3.7 ± 0.3 mb from a linear interpolation between the 735- and 970-MeV points. By using this estimate, the cross section σ_{01} was determined to be $0.1^{+0.5}_{-0.1}$ mb. This result is compared to a previous compilation of σ_{01} data in Table VI.[1] This table also lists the total cross sections for pion production from the interactions of nucleons in the $T=0$ and $T=1$ states ($\sigma(T=0)$ and $\sigma(T=1)$]. These cross sections were evaluated from the relations $\sigma(T=0)=3\sigma_{01}$ and $\sigma(T=1)=\sigma_{10}(np)+\sigma_{01}(d)+2\sigma_{11}$.

It was possible to estimate the angular variation of $d\sigma_{01}/d\Omega^*$ by using the relation $(d\sigma_{01}/d\Omega^*)(\theta^*)=[(d\sigma_{\pi^+}/d\Omega^*)(\theta^*)+(d\sigma_{\pi^-}/d\Omega^*)(\theta^*)-(d\sigma_{11}/d\Omega^*)(\theta^*)]$.[28] The angular distribution of $d\sigma_{11}/d\Omega^*$ was found by Cence *et al.*[25] to have the form $[230+82\cos^2(\theta^*)+92\cos^4(\theta^*)]$ μb/sr at 735 MeV. Use of this function in the expression for $d\sigma_{01}/d\Omega^*$ would have resulted in a negative (and thus unphysical) coefficient of $\cos^4(\theta^*)$, since the present data had no such term. However, Cence

TABLE VI. A summary of data concerning the reaction $np\to NN\pi^+$.

Neutron energy (MeV)	440	585	600	780	790
$\sigma(np\to NN\pi^\pm)$ mb	0.187 ± 0.015	1.3 ± 0.2	1.68 ± 0.17	~2.4	1.92 ± 0.20
σ_{11} (mb)	0.200 ± 0.020	1.72 ± 0.12	2.00 ± 0.12	~3.6	3.7 ± 0.3
σ_{01} (mb)	0.174 ± 0.035	0.9 ± 0.4	1.36 ± 0.36	$1.2^{+1.8}_{-0.9}$	$0.1^{+0.5}_{-0.1}$
$\sigma(T=1)$ (mb)	~3	~10	~11	~20	~20
$\sigma(T=0)$ (mb)	0.52 ± 0.10	2.7 ± 1.2	4.1 ± 1.2	$3.6^{+5.4}_{-2.7}$	$0.3^{+1.5}_{-0.3}$

et al. found that the funtion $[218+173\cos^2(\theta^*)]$ μb/sr represented their data nearly as well as the polynomial containing the $\cos^4(\theta^*)$ term. The coefficients 218 and 173 in this function were increased by the ratio of the $\sigma_{11_{790\,MeV}}/\sigma_{11_{735\,MeV}}$ which is just $\sim 3.7/3.46$ and then incorporated into the expression for $d\sigma_{01}/d\Omega^*$. This adjustment yielded the result

$$\frac{d\sigma_{01}}{d\Omega^*}(\theta^*) \cong [10^{+50}_{-10}+(0^{+20}_{-0})\cos^2(\theta^*)]\,\mu\text{b/sr} .$$

E. Comparison of results to previous data and an isobar-model calculation

It is of interest to compare the present results to those of previous experiments. Dzhelepov *et al.*[5] found that the peaks of their c.m.s. kinetic-energy spectra were located at about 0.60 $T^*_{\max}$, where $T^*_{\max}$ is the maximum pion kinetic energy. The peaks of the spectra in the present experiment appear to vary between about 0.55 to 0.65 $T^*_{\max}$. Yodh[3] found substantial asymmetries in the spectra of positive and negative pions around 400-MeV incident neutron energy. Dzhelepov *et al.*[5] also found asymmetries, although these were attributed to the effects of low-energy beam neutrons ($\sim$400 MeV). Dzhelepov *et al.*[5] and Kazarinov *et al.*[6] found the pion angular distributions of $d\sigma/d\Omega^*$ and $d\sigma_{01}/d\Omega^*$ to be of the form $a_0+a_2\cos^2(\theta^*)$. This is in agreement with the present data. Yodh[3] and Handler[4] found $d\sigma/d\Omega^*$ to vary as $a_0+a_1\cos(\theta^*)+a_2\cos^2(\theta^*)$. Unfortunately, not enough data were gathered by Rushbrook *et al.*[7] for an accurate determination of $d\sigma/d\Omega^*(\theta^*)$. The values of σ_{01} and $\sigma(np\to NN\pi^\pm)$ were previously compared in Table VI.

It was concluded by Cence *et al.*[25] that the majority of pions produced from the reaction $pp\to pp\pi^0$ at 735 MeV came from decaying isobars. These experimenters based their conclusion on the good agreement of their data with the Lindenbaum and Sternheimer isobar model.[29] A comparison of this isobar model to the present data was expected to show the effects of any $T=0$ pion production, based on the results of the Cence experiment. Such a comparison is most easily accomplished by calculating the quantity $d\sigma/dT^*$, as was done by Cence *et al.* This cross section is independent of the isobar angular distribution and any isobar polarization. Figure 8 shows $d\sigma/dT^*$ along with an isobar-model calculation, and three-body Lorentz-invariant phase space. Error bars on the data points reflect the uncertainties associated with the cross-section measurements as given in Table I. The dotted line includes extrapolated data. Both the isobar and phase-space curves were generated with the Berkeley program SAGE,[30,31] and are normalized to the same total cross section as the data. The SAGE isobar calculation was used to represent the predictions of the Lindenbaum and Sternheimer model. It can be seen that the isobar model does not reproduce the shape of our data. This may be due to the inadequacy of this simple model at this energy or possibly to the effects of $T=0$ pion production. It is interesting to note that the locations of $d\sigma/dT^*_{\max}$ in the present and Cence data are also different (0.6 $T^*_{\max}$ versus $\sim$0.7 $T^*_{\max}$). Dzhelepov *et al.*[5] also determined that their pion spectra were shifted towards lower energies when compared to π^0 spectra.

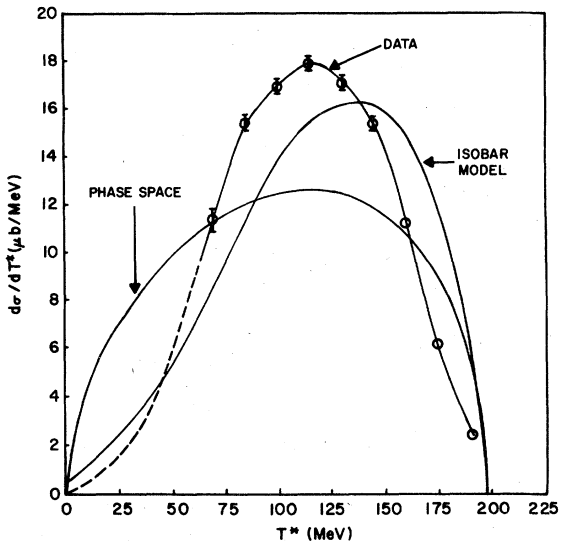

FIG. 8. Comparison of the data with an isobar calculation and phase space.

V. CONCLUSIONS

To summarize, our experimental data have been used to search for $T=0$ effects in pion production at 790 MeV. Four tests were made, with the following results.

(1) $\sigma(T=0)$ is less than 1.8 mb. This test is an insensitive one since $\sigma(T=0)=3[2\sigma(np\to NN\pi^\pm)-\sigma(pp\to pp\pi^0)]$ involves the subtraction of two nearly equal experimental values.

(2) Pion angular distributions integrated over energy show no front-back difference in the c.m.s.

which suggests an absence of $T=0$ amplitudes. However, in principle, the $T=0$ amplitudes could be present but not have the proper phase to interfere with $T=1$ amplitudes, resulting in the observed zero asymmetry.

(3) It was demonstrated that the data and an isobar-model calculation were significantly different. However, it is not possible to determine conclusively if this disagreement arises from the presence of $T=0$ amplitudes in the data, or because the $T=1$ amplitudes are not predicted properly by this model.

(4) The π^+ and π^- energy spectra at constant angle in the c.m.s. have a different shape for $\theta^* \lesssim 57°$, which is statistically significant and leads to the asymmetries in Table III. This suggests evidence for the presence of $T=0$ amplitudes.

---

*Present address: Science and Engineering Associates, Inc., Albuquerque, NM.
†Present address: Los Alamos Scientific Laboratory, Los Alamos, NM.
‡Present address: Science Applications Inc., LaJolla, CA.
§Present address: EG&G Inc., Los Alamos, NM.

[1]W. O. Lock and D. F. Measday, *Intermediate Energy Nuclear Physics* (Methuen, New York, 1970).
[2]S. Mandelstam, Proc. R. Soc. London A244, 491 (1958).
[3]G. B. Yodh, Phys. Rev. 98, 1330 (1955).
[4]R. Handler, Phys. Rev. B138, 1230 (1965).
[5]V. P. Dzhelepov, V. S. Kiselev, K. O. Oganesyan, and V. B. Flyagin, Zh. Eksp. Teor. Fiz. 50, 1491 (1966) [Sov. Phys.—JETP 23, 993 (1966)].
[6]Yu. M. Kazarinov and Yu. N. Siminov, Yad. Fiz. 4, 139 (1966) [Sov. J. Nucl. Phys. 4, 100 (1967)].
[7]J. G. Rushbrooke, D. V. Bugg, A. J. Oxley, J. A. Zoll, M. Jobes, J. Kinson, L. Riddiford, and B. Tallini, Nuovo Cimento 33, 1509 (1964).
[8]U. Amaldi, Jr., Rev. Mod. Phys. 39, 649 (1967).
[9]E. Ferrari and F. Selleri, Nuovo Cimento 27, 1450 (1963).
[10]G. Glass, Mahavir Jain, M. L. Evans, J. C. Hiebert, L. C. Northcliffe, B. E. Bonner, J. E. Simmons, C. Bjork, P. Riley, and C. Cassapakis, Phys. Rev. D 15, 36 (1977).
[11]T. Rupp, Ph.D. Dissertation, University of New Mexico, 1978 (unpublished).
[12]C. W. Bjork, P. J. Riley, B. E. Bonner, J. E. Simmons, K. D. Williamson Jr., M. L. Evans, G. Glass, J. C. Hiebert, M. Jain, R. A. Kenefick, L. C. Northcliffe, C. G. Cassapakis, H. C. Bryant, B. D. Dieterle, C. P. Leavitt, D. M. Wolfe, and D. W. Werren, Phys. Lett. 63B, 31 (1976).
[13]C. G. Cassapakis, H. C. Bryant, B. D. Dieterle, C. P. Leavitt, D. M. Wolfe, B. E. Bonner, J. E. Simmons, C. W. Bjork, P. J. Riley, M. L. Evans, G. Glass, J. C. Hiebert, M. Jain, R. A. Kenefick, L. C. Northcliffe, and D. W. Werren, Phys. Lett. 63B, 35 (1976).
[14]M. L. Evans, Ph.D. Dissertation, Texas A&M University, 1976 (unpublished).
[15]H. Hinterberger and R. Winston, Rev. Sci. Instrum. 37, 1094 (1966).
[16]D. Brown, Nucl. Instrum. Methods 117, 561 (1974).
[17]L. R. Biswell and R. E. Rajala, Los Alamos Sci. Lab Report No. LA-4916-MS, 1972 (unpublished).
[18]J. C. Hiebert and A. C. Niethammer, Los Alamos Sci. Lab Report No. LA-5609-MS, 1974 (unpublished).
[19]M. Jain, D. Werren, and H. Bryant (unpublished).
[20]M. Hutchinson, J. Friedman, and A. Rittenberg, Group A Programming Note No. P-171, Univ. Of California, LBL, Berkely, California, 1973 (unpublished).
[21]D. R. F. Cochran, P. N. Dean, P. A. M. Gram, E. A. Knapp, E. R. Martin, D. E. Nagle, R. B. Perkins, W. J. Shlaer, H. A. Thiessen, and E. D. Theriot, Phys. Rev. D 6, 3085 (1972).
[22]M. Jain (private communication).
[23]R. J. N. Phillips, Nucl. Phys. B53, 650 (1964).
[24]P. R. Bevington, *Data Reduction and Error Analysis for the Physical Sciences* (McGraw-Hill, New York, 1969).
[25]R. J. Cence, D. L. Lind, G. D. Mead, and B. J. Moyer, Phys. Rev. 131, 2713 (1963).
[26]I. S. Hughes, P. V. March, H. Muirhead, and W. O. Lock, Philos. Mag. 2, 215 (1957).
[27]A. P. Batson, B. B. Culwick, J. G. Hill, and L. Riddiford, Proc. R. Soc. London A251, 218 (1959).
[28]L. Van Hove, R. Marshak, and A. Pais, Phys. Rev. 88, 1211 (1952).
[29]S. J. Lindenbaum and R. M. Sternheimer, Phys. Rev. 105, 1874 (1957).
[30]J. Friedman, Group A Programming Note No. P-189, Univ. of California, LBL, Berkeley, California, 1969 (unpublished).
[31]J. Friedman, LBL Report No. URCL-19206, 1970 (unpublished).

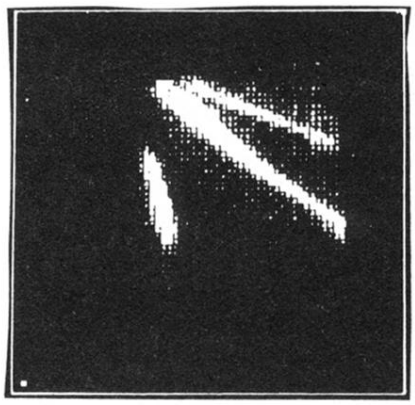

FIG. 3. On-line plot of particle momentum vs TOF.